INAF-Osservatorio astrofisico di Torino
Technical Report nr. 167

Simulation of Visible Light and UV images for the METIS coronagraph

Alessandro Bemporad

Pino Torinese, 9 ottobre 2014

Simulation of Visible Light and UV images for the METIS coronagraph

A. Bemporad
INAF-Osservatorio Astronomico di Torino, via Osservatorio 20,
10025 Pino Torinese (TO), Italy; bemporad @oato.inaf.it

ABSTRACT

This report describes step by step how the simulated images of METIS instrument expected on the CCD detector have been constructed. In summary, the images are built for both channels (UV and VL) starting from images of white light corona acquired during total solar eclipses and rescaling those images with HI Lyman-α intensities measured by SOHO/UVCS instrument at different heliocentric distances and latitudes and similar measurements provided in the literature for VL intensities. A routine has been written (in IDL language) able to provide UV and VL images for any heliocentric distance of the Solar Orbiter spacecraft and for both the minimum and maximum phases of the solar cycle. Simulated images have then been used to estimate the expected counts number and the exposure times required to have a provided signal to noise ratio on both the UV and VL channels. This report is a revision and extension of work already described in a previous Technical Report (OATo Tech.Rep. 132, 03-06-2010), dealing only with the UV channel.

Summary

Index of Figures

Index of Tables

1. SUMMARY OF INPUT INSTRUMENTAL PARAMETERS

The METIS simulated images described here have been obtained by assuming directly the instrument effective areas (cm^2) provided in a previous document (OATo Tech.Rep. 132, 03-06-2010). These effective areas are provided again below (*Figure 1* and *Table 1*) for the reader convenience: description of reference METIS instrumental parameters are provided in that document and previous documentation.

Field of view [°]	Vignetting Fraction	Geometrical Area [cm^2]	Effective areas [cm^2]	
			VL	UV
1.5	0.024	0.298	1.16e-02	6.85e-03
1.8	0.112	1.407	5.47e-02	3.24e-02
2.1	0.224	2.814	1.09e-01	6.47e-02
2.4	0.343	4.310	1.68e-01	9.91e-02
2.7	0.463	5.815	2.26e-01	1.34e-01
2.9	0.573	7.190	2.80e-01	1.65e-01

Table 1: Effective areas of the VL and UV imaging paths as a function of angular FoV

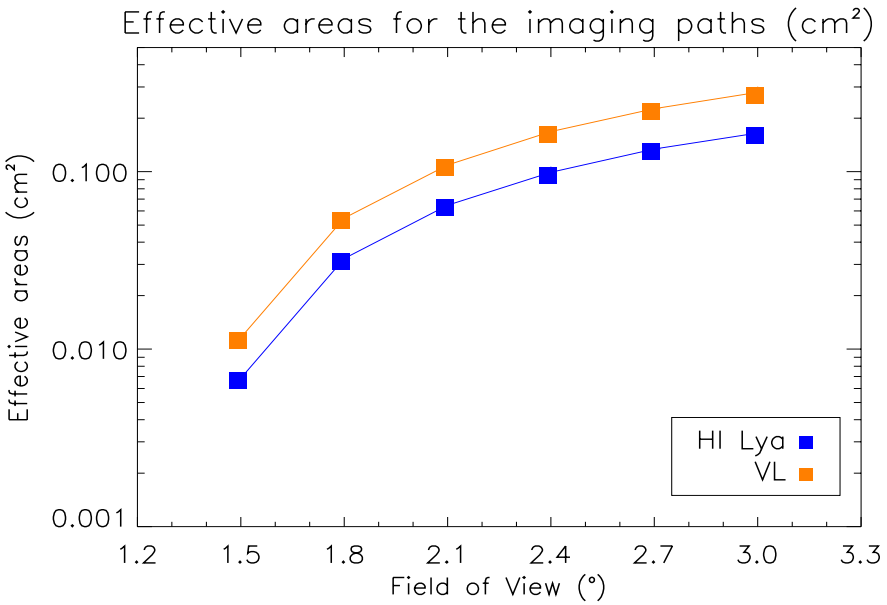

Figure 1: Estimated effective areas of the VL and UV imaging paths as a function of angular FoV

2. INPUT IMAGES, INTENSITIES AND SPECTRA

The input white light coronagraphic images used in the previous report were composite MarkIV + LASCO C2 + LASCO C3 images. Nevertheless, these composite images have clear discontinuities at the edges of the field of view of each instrument. For this reason, images described here have been obtained starting from eclipse observations of the solar corona: these images have the advantage to have a very broad field of view observed with a single instrument. In particular, input images are total solar eclipse observations (wide field of view) acquired in visible light by Dr. M. Druckmuller in 1997[1] (*Figure 2*, left) and 2012[2] (*Figure 2*, right), in order to have an image representative of coronal conditions during the minimum and maximum phases of solar activity, respectively.

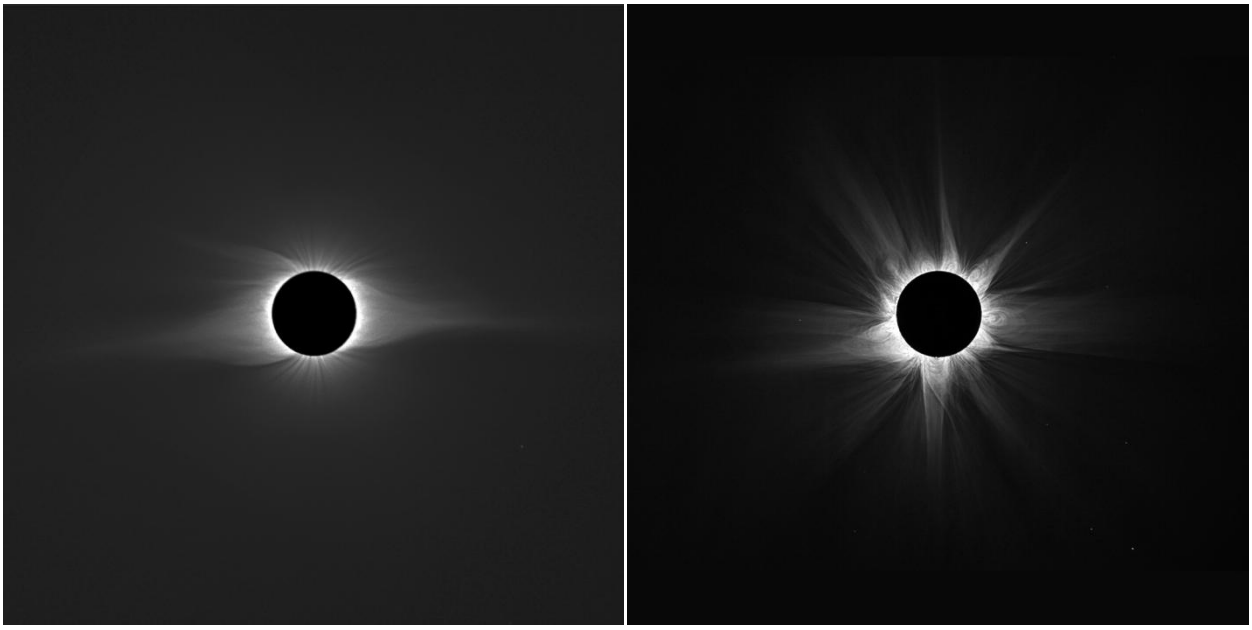

Figure 2: input total solar eclipse images for the solar minimum (left) and solar maximum (right) conditions.

These images have been filtered by the author to enhance the contrast and visibility of faint coronal structures, hence the visibility of such structures in real METIS images will be different. In any case this is not a problem because the aim of METIS simulated images is simply to mimic the general appearance of solar corona and in particular the distribution of large scale structures like coronal streamers. In any case these images have an approximate spatial resolution of about 10.9"/pixel, hence very close to the METIS spatial resolution by 10"/pixel (in the VL channel).

As already done in the previous analysis, input UV HI Lyman-α intensities (phot cm^{-2} s^{-1} sr^{-1}) have been assumed from UVCS data observations. In particular, I assumed the integrated line intensity profiles vs. altitude provided in the "Counts rate Estimates – METIS Instrument Performance" document (issue 2, rev.2, 11/12/2007). A power law fitting to the profiles provided in this document (shown in *Figure 3*) yields the following analytic expressions for the H Lyman-α line intensity (phot cm^{-2} s^{-1} sr^{-1}) as a function of the heliocentric distance h (measured in units of R_{sun} , see Fig. 2) at the equatorial (I_{eq}) and polar (I_{po}) regions for the minimum and maximum phases of solar activity cycle:

[1] http://www.zam.fme.vutbr.cz/~druck/eclipse/Ecl1997r/0-info.htm
[2] http://www.zam.fme.vutbr.cz/~druck/eclipse/Ecl2012a/0-info.htm

$$I_{eq,\min}(Ly\alpha) = 4.85\times10^{10}\left(\frac{518.56}{h^{11.07}}+\frac{32.17}{h^{5.1}}+\frac{1.29}{h^{2.32}}\right);\quad I_{po,\min}(Ly\alpha) = 2.04\times10^{9}\left(\frac{2155.27}{h^{10.77}}+\frac{128.98}{h^{6.73}}\right)$$

$$I_{eq,\max}(Ly\alpha) = 1.72\times10^{10}\left(\frac{2258.13}{h^{6.807}}+\frac{6.903}{h^{2.197}}\right)\quad;\quad I_{po,\max}(Ly\alpha) = 2.63\times10^{9}\left(\frac{3194.05}{h^{7.996}}+\frac{262.17}{h^{3.92}}\right)$$

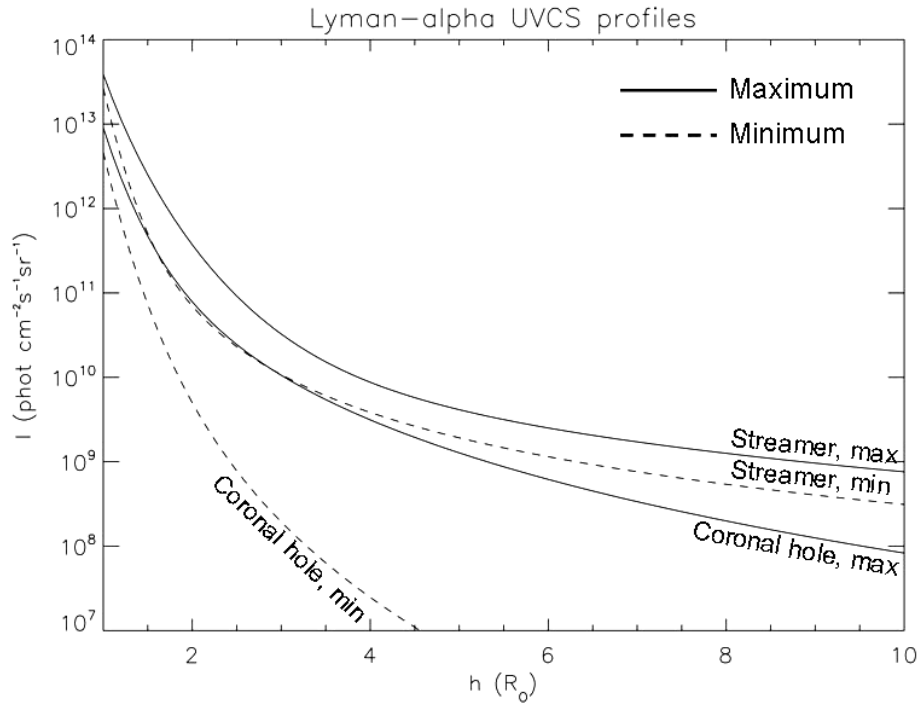

Figure 3: example of input Lyman-α intensity profiles measured by UVCS (see text).

The interplanetary HI Lyman-α intensity has been also taken into account and a constant value by I_{inter} = 3×10^{7} phot cm^{-2} s^{-1} sr^{-1} (Kohl et al. 1997) has been added to all pixels to the above intensities as a simple background.

The input VL intensities (phot cm^{-2} s^{-1} sr^{-1}) have been assumed from Allen (2000), whose intensities provided for the K- and F-corona for maximum and minimum phase of the solar cycle have been fitted with power laws. Resulting curves (shown in *Figure 4*) are given below in log scale of the intensity:

$$Log(I_{K,\max}) = \frac{5.376}{h^{0.896}}+\frac{0.4657}{h^{0.9145}}\quad;$$

$$Log(I_{K,eq,\min}) = \frac{6.716}{h^{0.6825}}-\frac{0.0306}{h^{2.0298}}\quad;\quad Log(I_{F,eq}) = \frac{2.419}{h^{0.7903}}-\frac{0.9057}{h^{0.7635}}$$

$$Log(I_{K,po,\min}) = \frac{6.906}{h^{0.6970}}+\frac{0.4722}{h^{13.9580}}\quad;\quad Log(I_{F,po}) = \frac{2.4754}{h^{0.9219}}-\frac{0.9609}{h^{0.9185}}$$

The above curves have been computed starting form a total visible light brightness of the Sun disk integrated between 600 – 650 nm (using values given by Allen 2000, "*Astrophysical quantities*", p. 354), which is a good approximation for the METIS band-pass interval (580 – 640 nm). The resulting value for total solar disk brightness used in this work is B_{sun} = 3.8×10^{20} phot cm^{-2} s^{-1} sr^{-1}.
All the above intensities shown in *Figure 3* and *Figure 4* are also in agreement with those reported in the previous "Coronal Radiances and Modelling" report (METIS-OACT-TNO-004, issue 2, rev. 0, 22.7.2013).

Effective area images of the METIS instrument have been built starting from values provided in *Table 1* and *Figure 1* and by simply assuming symmetry about the optical axis: resulting images for VL (top) and UV (bottom) channels are shown in *Figure 5* (units of cm^2).

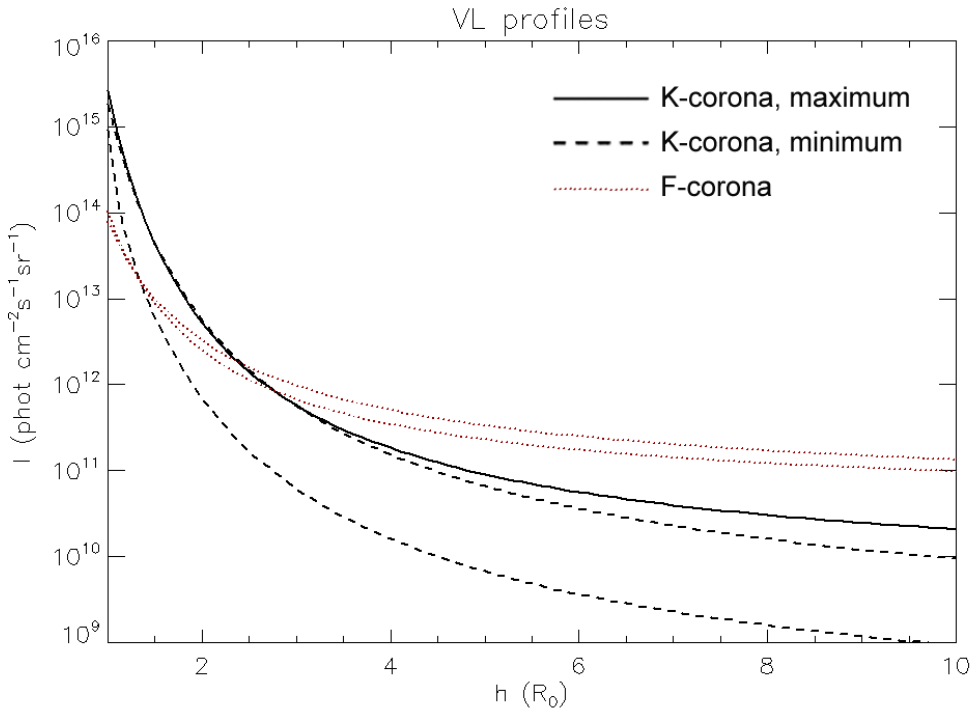

Figure 4: VL intensity profiles for the K-corona at solar maximum (solid black line), K-corona at solar minimum at the equator and at the pole (black dashed lines) and F- corona at the equator and at the pole (red dotted lines).

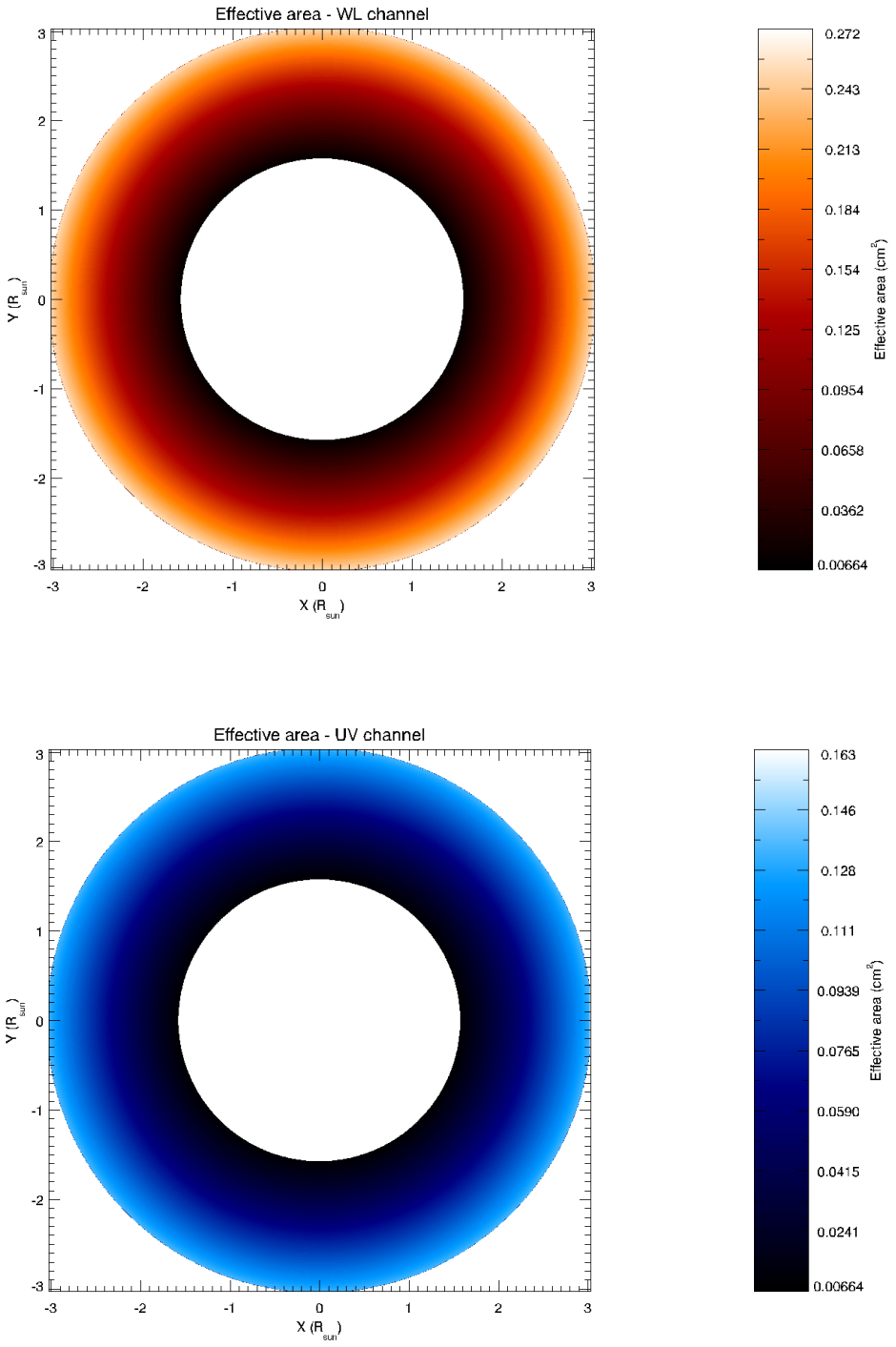

Figure 5: effective area images for the VL (top) and UV (bottom) METIS channels.

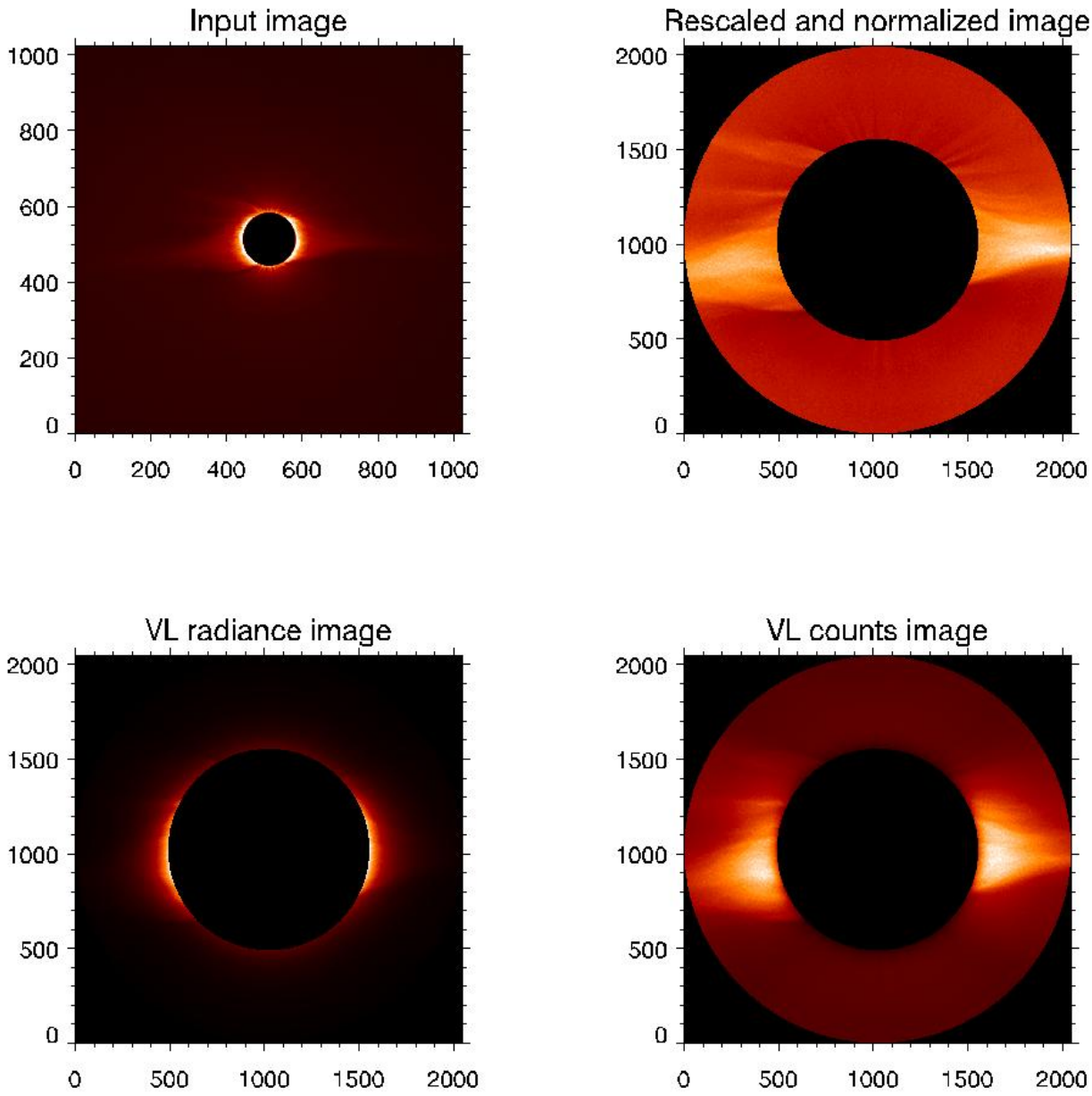

Figure 6: example of successive steps followed to build a VL intensity image; this example refers in particular to a spacecraft heliocentric distance of 0.28 AU.

3. BUILDING THE CORONAGRAPHIC IMAGES

The successive steps followed to build UV (HI Lyman-α) and VL (640-580nm) coronagraphic images are:

1. Convert the 1024×1024 white light eclipse image (*Figure 2* and *Figure 6*, top left) to a 2048×2048 pix^2 image with the correct METIS spatial resolution (km/pixel) and field of view for the actual heliocentric distance of the Solar Obiter spacecraft;
2. Normalize the white light image to the average radial intensity profile (obtained averaging over 90 radial profiles extracted from the input image, one profile each 4°);
3. Remove any signal outside the outer and inner edges of the METIS coronagraph field of view (*Figure 6*, top right);
4. Apply a trigonometric multiplying function $f(\theta)$ (where θ is the solar latitude), with $0 \leq f \leq 1$, to scale the 2-D normalized image to the UV and VL polar and equatorial intensities (*Figure 6*, bottom left).
5. Multiply the resulting UV and VL radiance images (phot cm^{-2} sr^{-1} s^{-1}) by the corresponding effective area image (cm^2) and the instrumental spatial scale Ω (sr pix^{-1}), to derive the counts image (*Figure 6*, bottom right),

where the instrument spatial scale Ω is given by $(10 \text{ arcsec})^2/\text{pixel} = 2.42\times10^{-9}$ (sr/pixel), for the VL imaging path, and $(20 \text{ arcsec})^2/\text{pixel} = 9.68\times10^{-9}$ (sr/pixel), for the UV imaging path in analogue mode. An example of VL image (units of counts s^{-1} $pixel^{-1}$) resulting from the above procedure is shown in *Figure 6* (bottom right). A similar image has been obtained with the same procedure described above for the UV channel (see Figures in the Appendix). In particular, in the radiance images the radial intensity profiles extracted above the pole or at the equator coincides with the UVCS intensity profiles at that latitudes for UV with the interplanetary contribution, and with the VL intensity profiles given by Allen (2000) with F-corona contribution, as it is shown in the top plots of *Figure 7* and *Figure 8* for a spacecraft distance of 0.28 AU and 0.50 AU, respectively. At mid latitudes the intensities are intermediate between polar and equatorial intensities. The resulting 2D image also mimic the presence of coronal structures, even if (as mentioned above) input total solar eclipse images are filtered in order to enhance the visibility of faint coronal structures.

Notice that the polar coronal hole intensity in the UV channel observed at 0.50 AU is not in agreement with the theoretical UVCS profile because of the interplanetary contribution (*Figure 8*, top left panel). Notice also that, because at large heliocentric distances the VL channel is dominated by the F-corona contribution and because its radial profile is much flatter than the K-corona profile, once the radiances are multiplied by the effective areas the resulting curve for the number of counts will have a minimum closer to the lower edge of the image and a maximum close to the outer edge (*Figure 8*, bottom right panel).

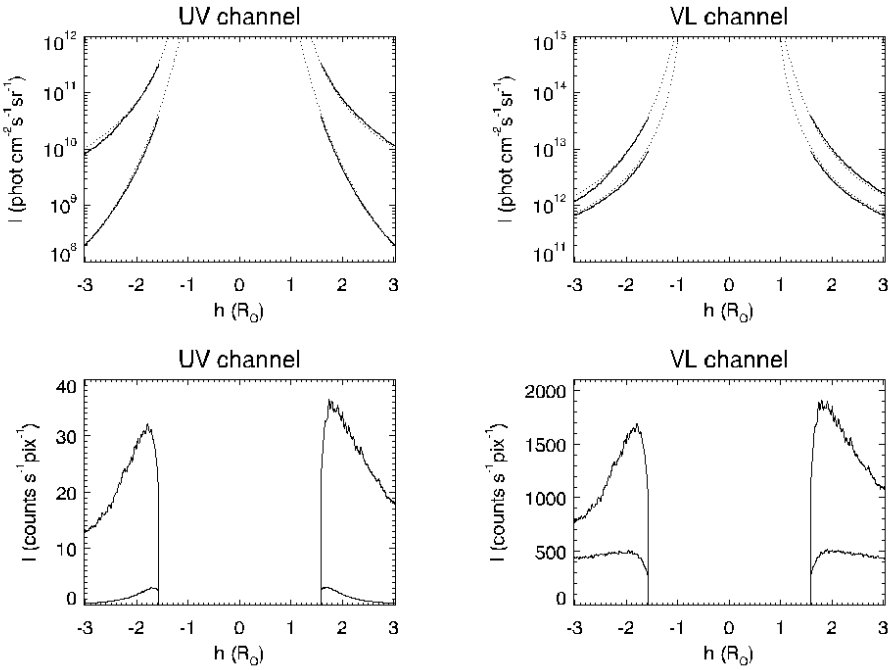

Figure 7, top: comparison between intensity values along an equatorial row and a polar column of the 2D simulated images (solid line) and the theoretical curves (dotted lines) for the UV (left) and VL (right) METIS channels at 0.28 AU for solar minimum. Bottom: resulting expected counts along an equatorial row and a polar column of the 2D METIS simulated images for the UV (left) and VL (right) METIS channels.

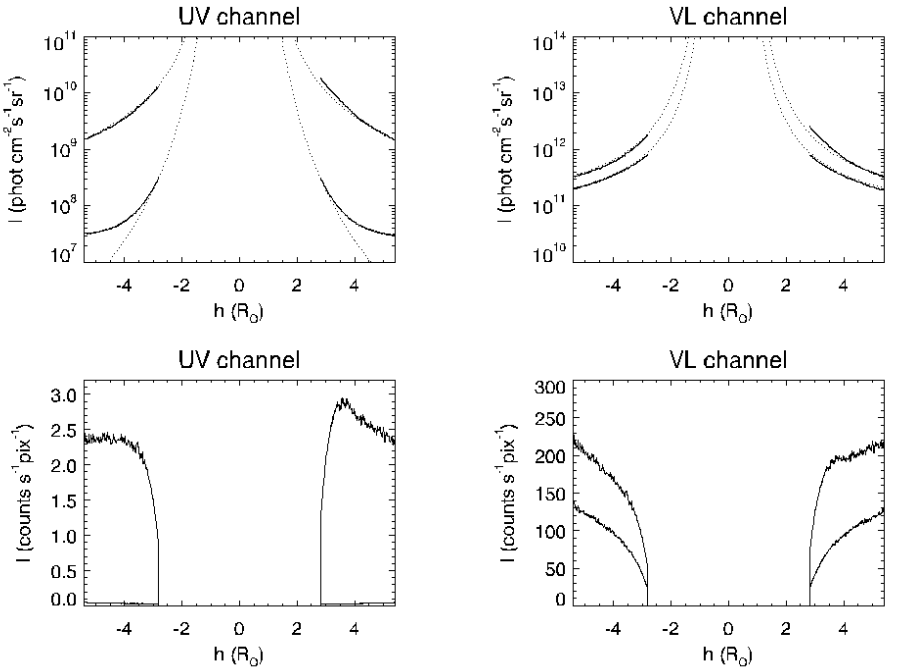

Figure 8, top: comparison between intensity values along an equatorial row and a polar column of the 2D simulated images (solid line) and the theoretical curves (dotted lines) for the UV (left) and VL (right) METIS channels at 0.50 AU for solar minimum. Bottom: resulting expected counts along an equatorial row and a polar column of the 2D METIS simulated images for the UV (left) and VL (right) METIS channels.

4. ESTIMATE OF REQUIRED EXPOSURE TIMES

The resulting images are in units of counts s^{-1} pix^{-1}; these images can then be used to estimate the exposure times t_{exp} required to have a fixed S/N (signal-to-noise) ratio it is possible to derive at each altitude. Required exposure times have been computed by assuming that the noise N is due only to the Poissonian statistic, i.e. $N = S^{1/2}$; hence $S/N = 10$ implies $S = 100$ counts. Given a fixed S/N ratio and a number of expected counts C_{line} (counts/s), the exposure time t_{exp} (s) required to have this S/N ratio for a single pixel is simply $t_{exp} = (S/N)^2 / C_{line}$.

Resulting exposure times computed for S/N = 10 when the spacecraft will be at a distance of 0.28 AU and 0.50 AU are provided in the Appendix for both channels at minimum and maximum of the solar activity cycle. In particular, images in the Appendix are provided with the following order

1. Intensity (counts) images at 0.28 AU:
    a. VL channel, solar minimum;
    b. UV channel, solar minimum;
    c. VL channel, solar maximum;
    d. UV channel, solar maximum;
2. Intensity (counts) images at 0.50 AU:
    a. VL channel, solar minimum;
    b. UV channel, solar minimum;
    c. VL channel, solar maximum;
    d. UV channel, solar maximum;
3. Exposure times (seconds) images at 0.28 AU:
    a. VL channel, solar minimum;
    b. UV channel, solar minimum;
    c. VL channel, solar maximum;
    d. UV channel, solar maximum;
4. Exposure times (seconds) images at 0.50 AU:
    a. VL channel, solar minimum;
    b. UV channel, solar minimum;
    c. VL channel, solar maximum;
    d. UV channel, solar maximum;

These images show mainly what follows:

1. At 0.28 AU exposure times longer than ~0.2 s and ~ 300 s will be required for solar minimum in order to have a good S/N ratio in polar coronal holes in the VL and UV channels, respectively; during solar maximum these times will relax down to ~0.1 s and ~5 s;
2. At 0.50 AU exposure times longer than ~3 s and ~3000 s will be required for solar minimum in order to have a good S/N ratio in polar coronal holes in the VL and UV channels, respectively; during solar maximum these times will relax down to ~1.5 s and ~80 s;
3. Closer to the Sun the most critical part for S/N ratio of the UV and VL images corresponds to the outer coronal region in the instrument field of view; on the contrary, farther form the Sun the coronal intensity profiles become flatter and the situation reverses, with the most critical part located in the inner section of the image.

Please notice that the above exposure times have been computed by neglecting any other possible source of noise (like read-out noise, dark current) or image contamination (stray light), and only Poissonian noise has been considered. For this reason, the above exposure times have to be considered as lower limits to the real required exposure times. Color scales in the intensity images have been adjusted to the maximum value of the whole array, while color scales in the exposure time images are kept constant in order to facilitate the comparison between different phases of solar cycle and different spacecraft distances.

Appendix

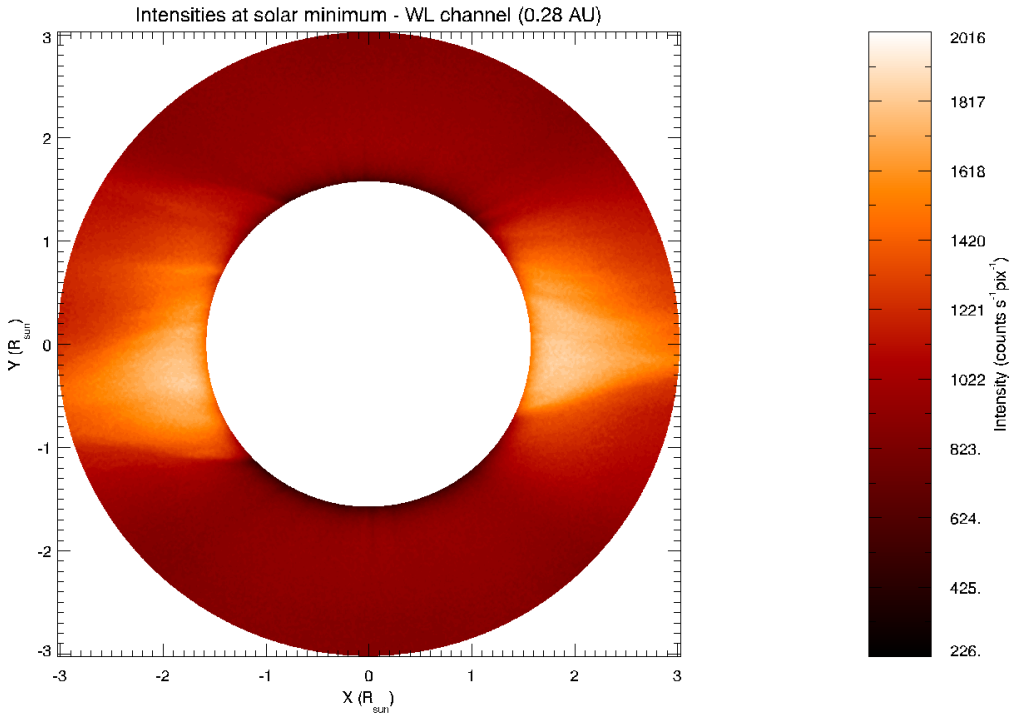
Intensities at solar minimum - WL channel (0.28 AU)
Y (R sun)
X (R sun)
3
2
1
0
-1
-2
-3
2016
1817
1618
1420
1221
1022
823.
624.
425.
226.
Intensity (counts s-1 pix-1)

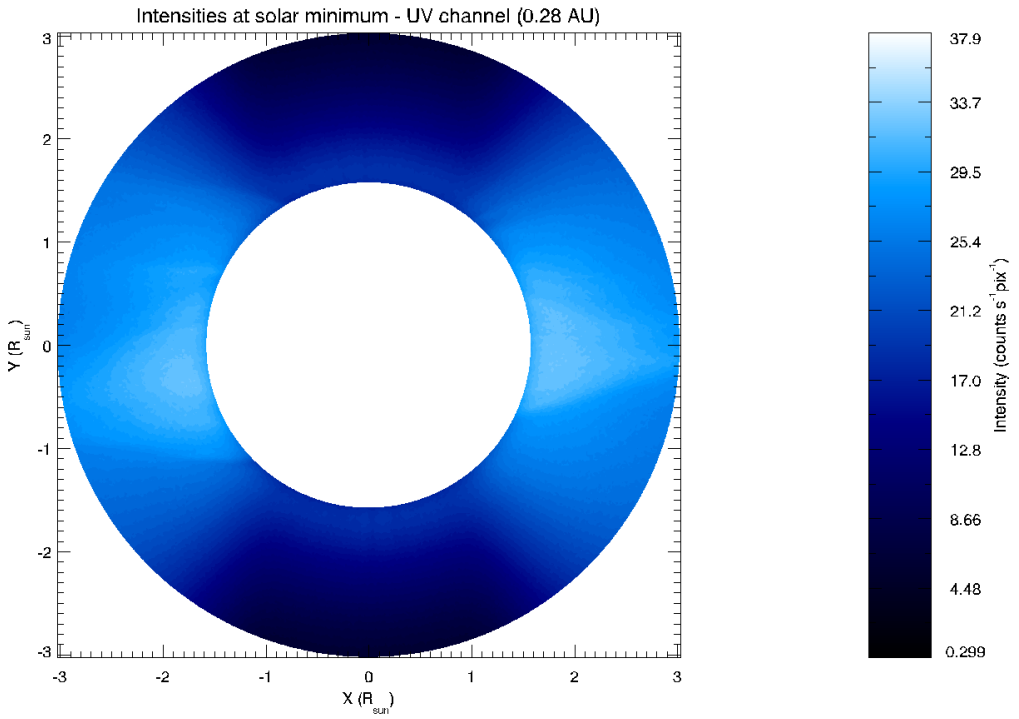
Intensities at solar minimum - UV channel (0.28 AU)
Y (R sun)
X (R sun)
3
2
1
0
-1
-2
-3
37.9
33.7
29.5
25.4
21.2
17.0
12.8
8.66
4.48
0.299
Intensity (counts s-1 pix-1)

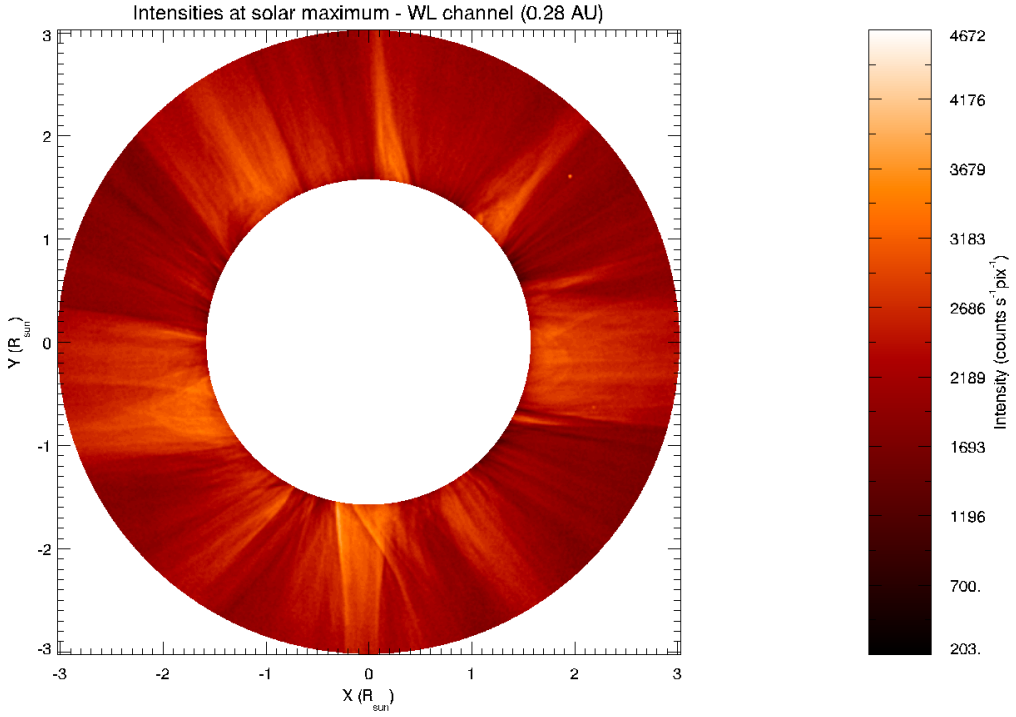
Intensities at solar maximum - WL channel (0.28 AU)
Y (R sun)
X (R sun)
3
2
1
0
-1
-2
-3
4672
4176
3679
3183
2686
2189
1693
1196
700.
203.
Intensity (counts s-1 pix-1)

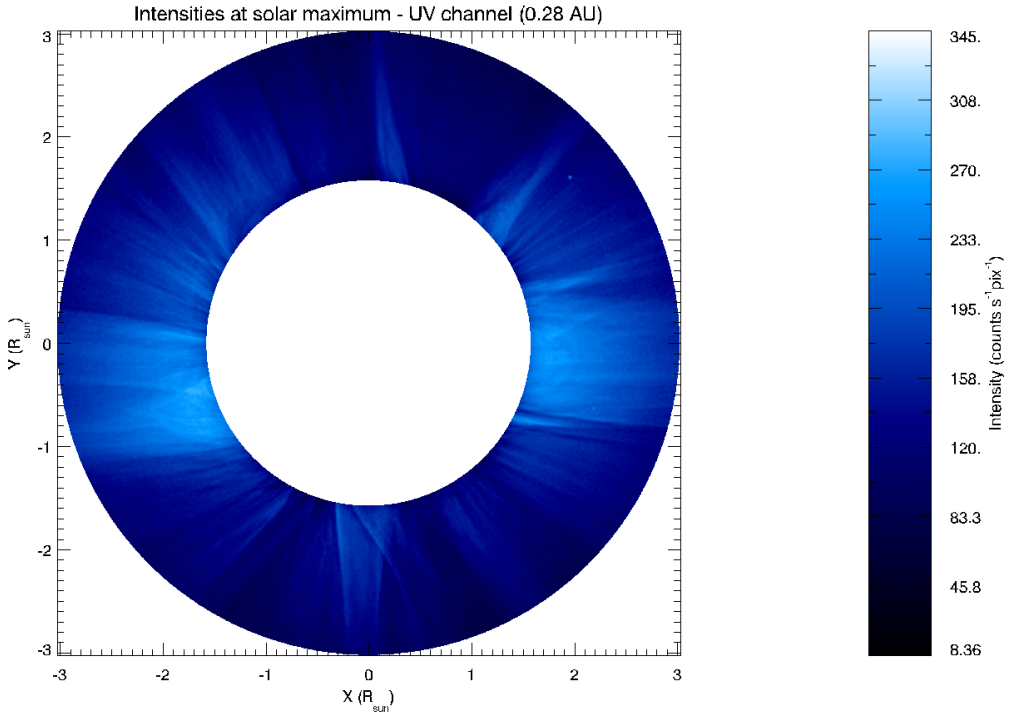
Intensities at solar maximum - UV channel (0.28 AU)
Y (R sun)
X (R sun)
3
2
1
0
-1
-2
-3
345.
308.
270.
233.
195.
158.
120.
83.3
45.8
8.36
Intensity (counts s-1 pix-1)

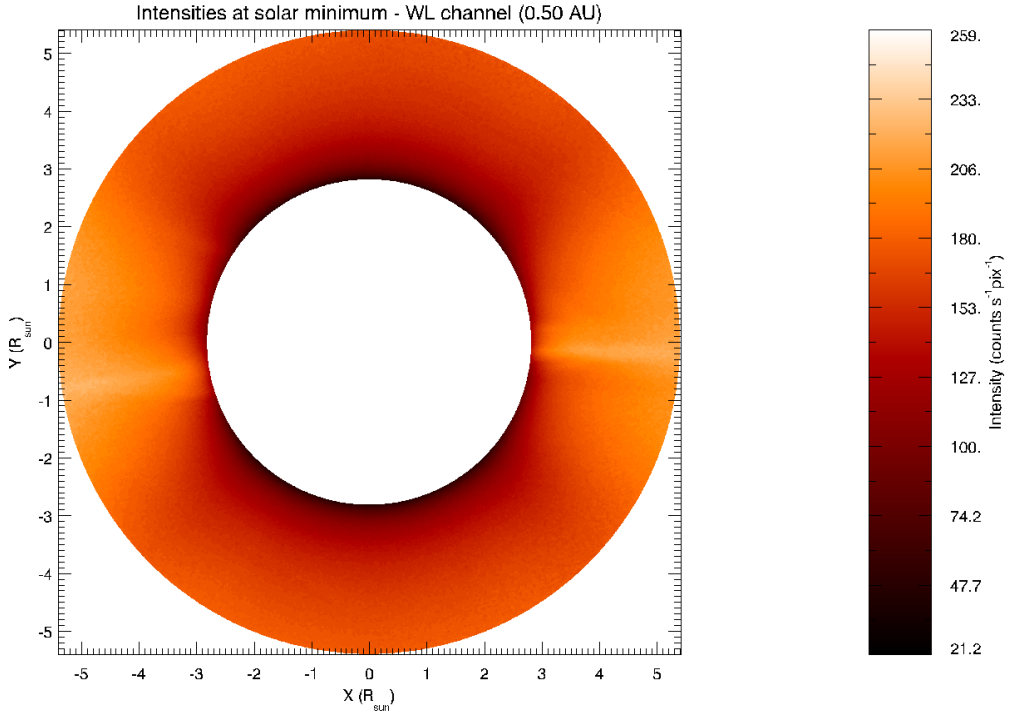
Intensities at solar minimum - WL channel (0.50 AU)
Y (R sun)
X (R sun)
Intensity (counts s-1 pix-1)
259.
233.
206.
180.
153.
127.
100.
74.2
47.7
21.2

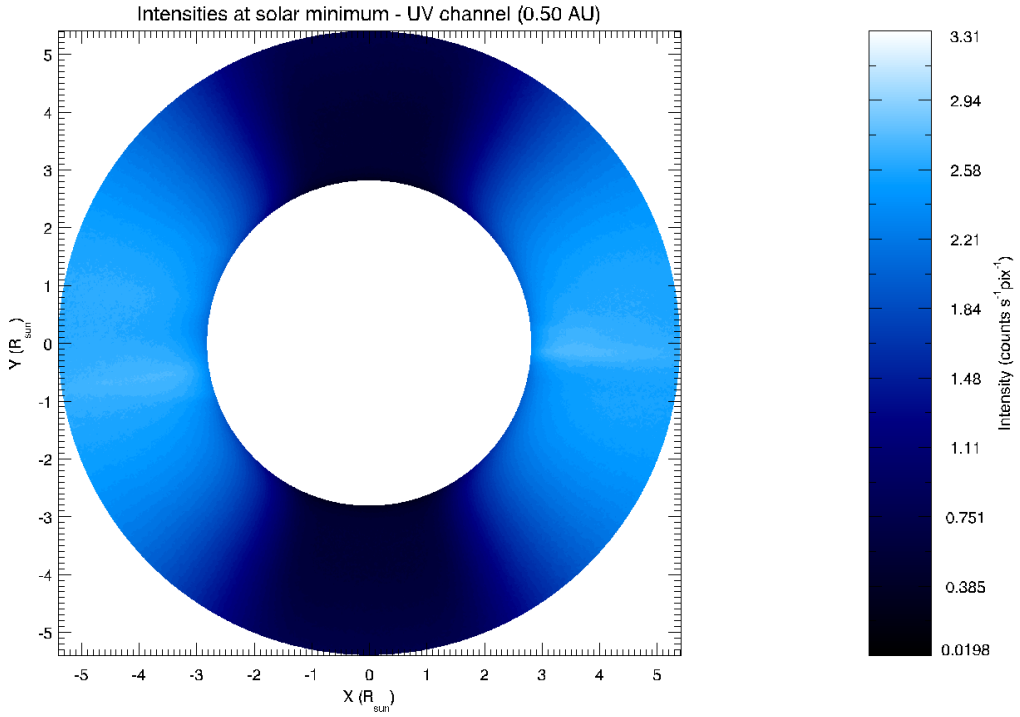
Intensities at solar minimum - UV channel (0.50 AU)
Y (R sun)
X (R sun)
Intensity (counts s-1 pix-1)
3.31
2.94
2.58
2.21
1.84
1.48
1.11
0.751
0.385
0.0198

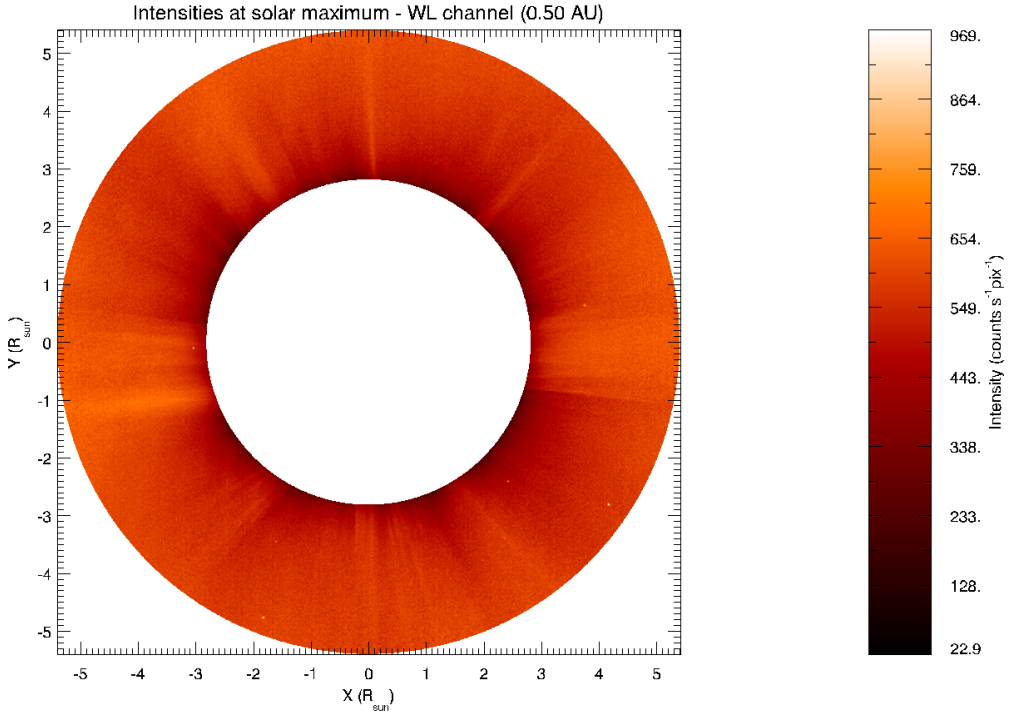
Intensities at solar maximum - WL channel (0.50 AU)
Y (R sun)
X (R sun)
Intensity (counts s-1 pix-1)
969.
864.
759.
654.
549.
443.
338.
233.
128.
22.9

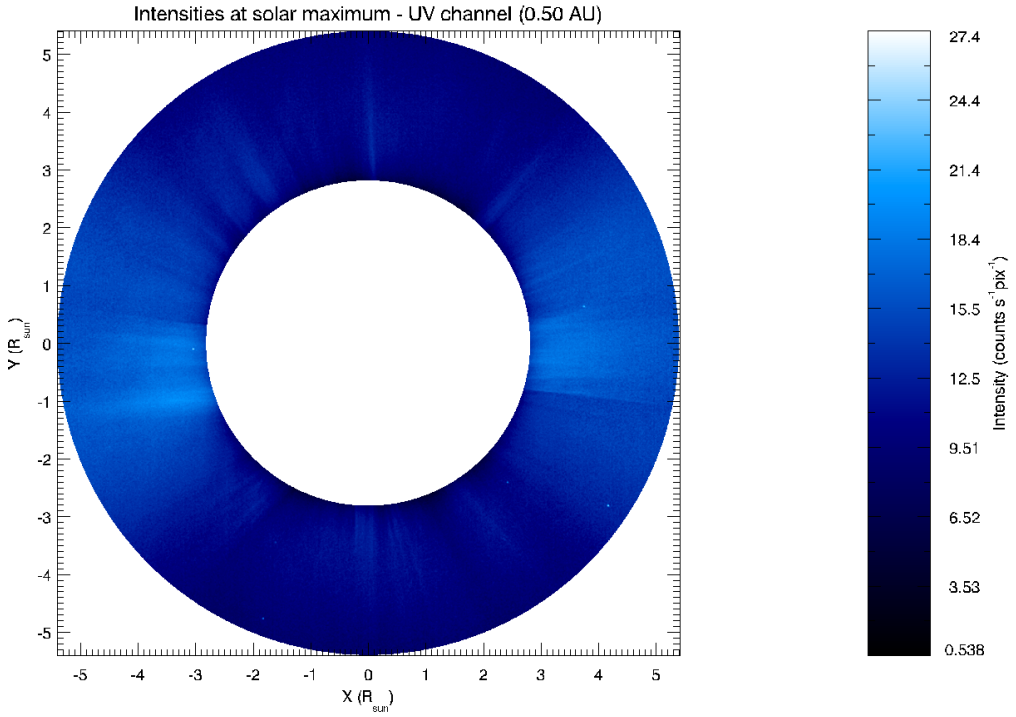
Intensities at solar maximum - UV channel (0.50 AU)
Y (R sun)
X (R sun)
Intensity (counts s-1 pix-1)
27.4
24.4
21.4
18.4
15.5
12.5
9.51
6.52
3.53
0.538

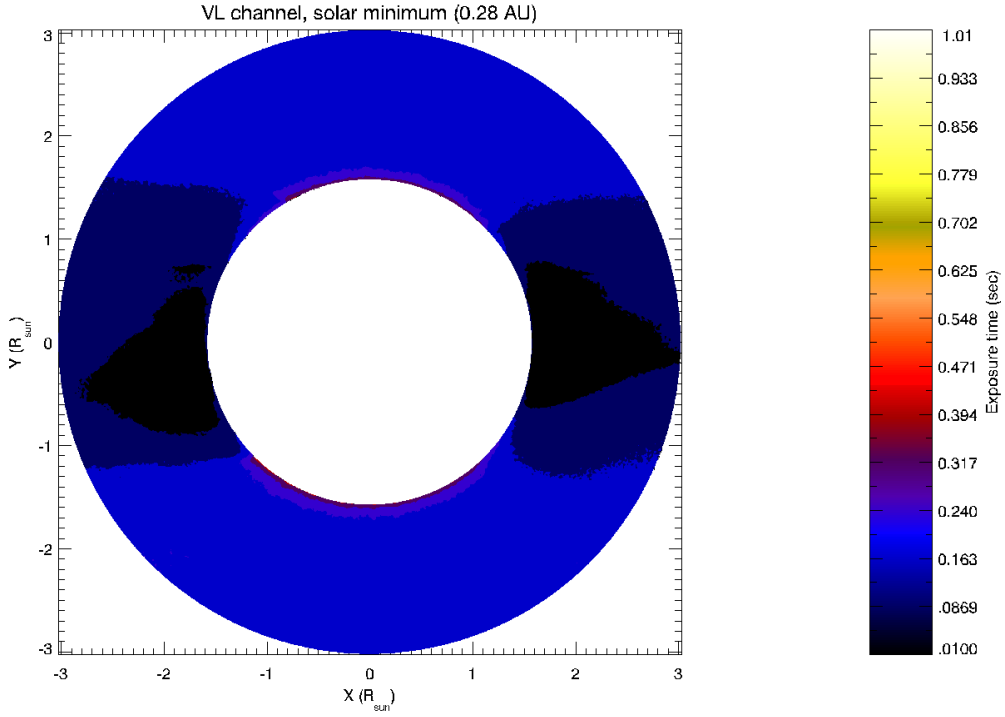
VL channel, solar minimum (0.28 AU)
Y (R sun)
X (R sun)
3
2
1
0
-1
-2
-3
1.01
0.933
0.856
0.779
0.702
0.625
0.548
0.471
0.394
0.317
0.240
0.163
.0869
.0100
Exposure time (sec)

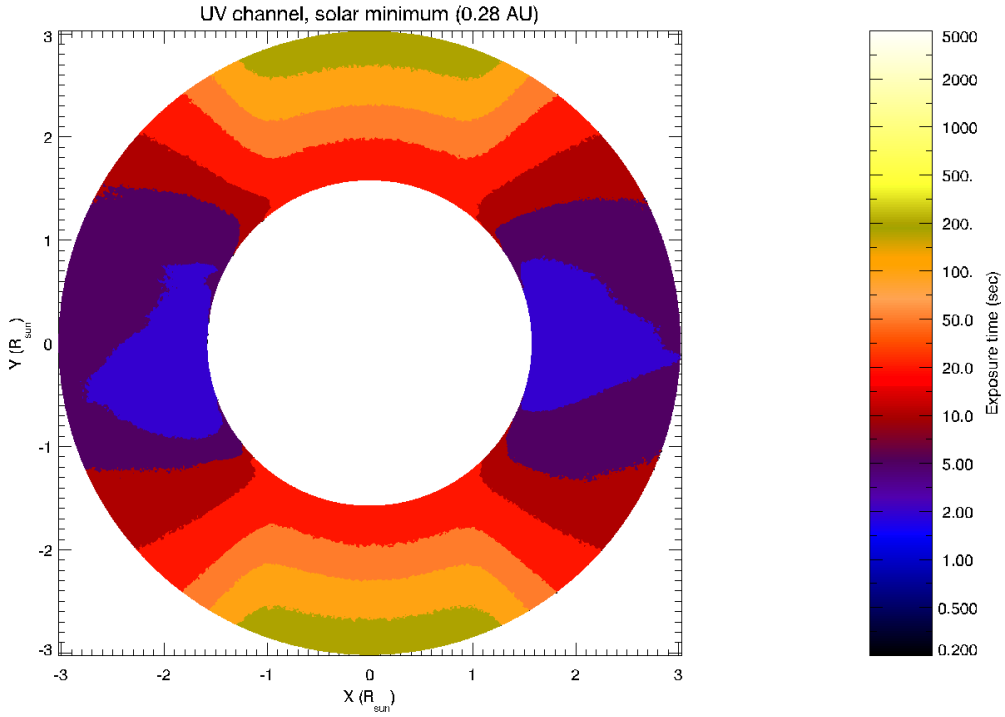
UV channel, solar minimum (0.28 AU)
Y (R sun)
X (R sun)
3
2
1
0
-1
-2
-3
5000
2000
1000
500.
200.
100.
50.0
20.0
10.0
5.00
2.00
1.00
0.500
0.200
Exposure time (sec)

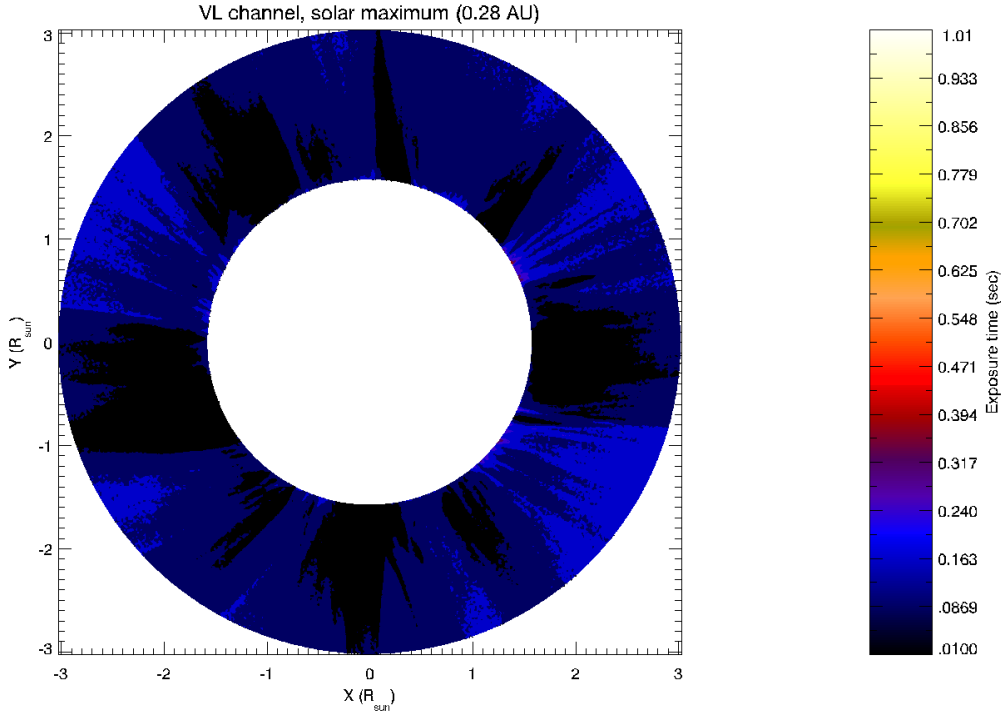
VL channel, solar maximum (0.28 AU)
Y (R sun)
X (R sun)
Exposure time (sec)
1.01
0.933
0.856
0.779
0.702
0.625
0.548
0.471
0.394
0.317
0.240
0.163
.0869
.0100

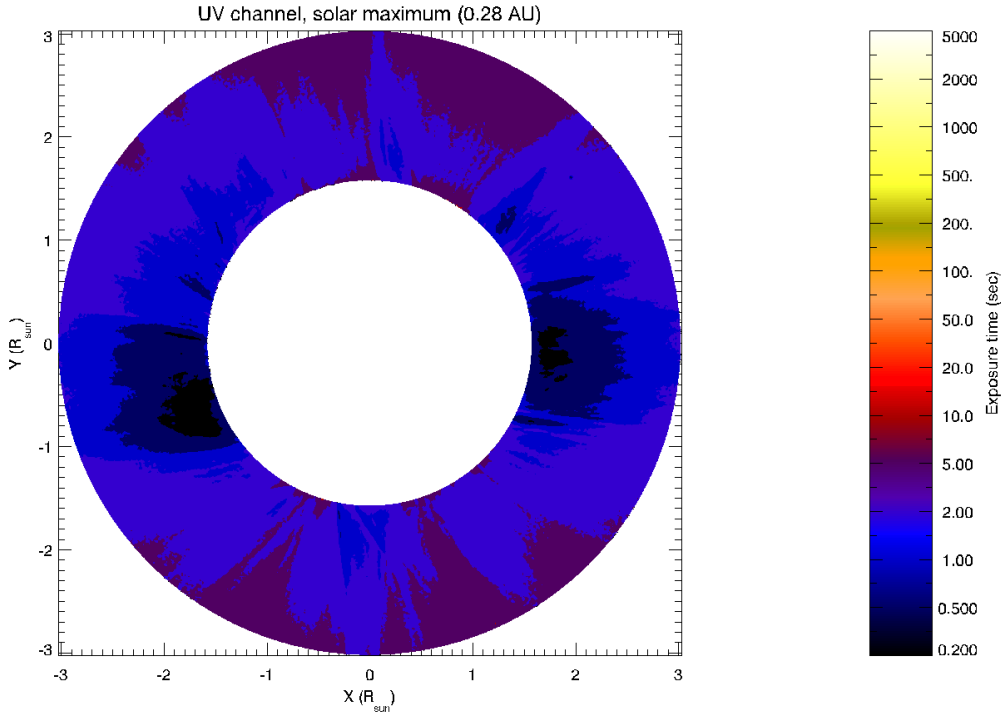
UV channel, solar maximum (0.28 AU)
Y (R sun)
X (R sun)
Exposure time (sec)
5000
2000
1000
500.
200.
100.
50.0
20.0
10.0
5.00
2.00
1.00
0.500
0.200

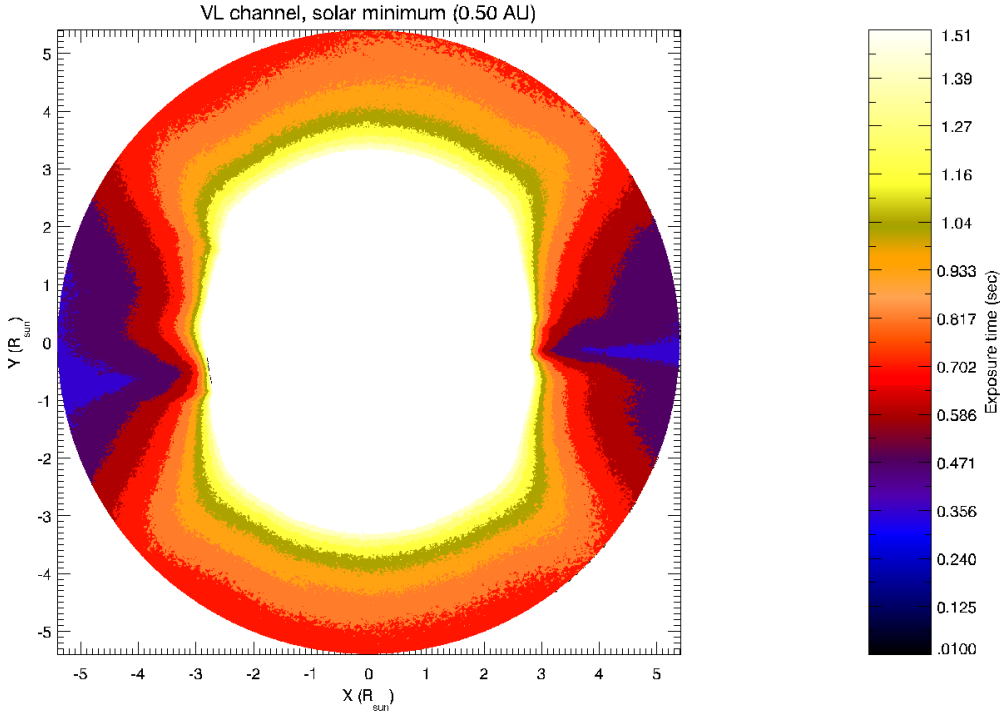
VL channel, solar minimum (0.50 AU)
Y (R sun)
X (R sun)
Exposure time (sec)
1.51
1.39
1.27
1.16
1.04
0.933
0.817
0.702
0.586
0.471
0.356
0.240
0.125
.0100

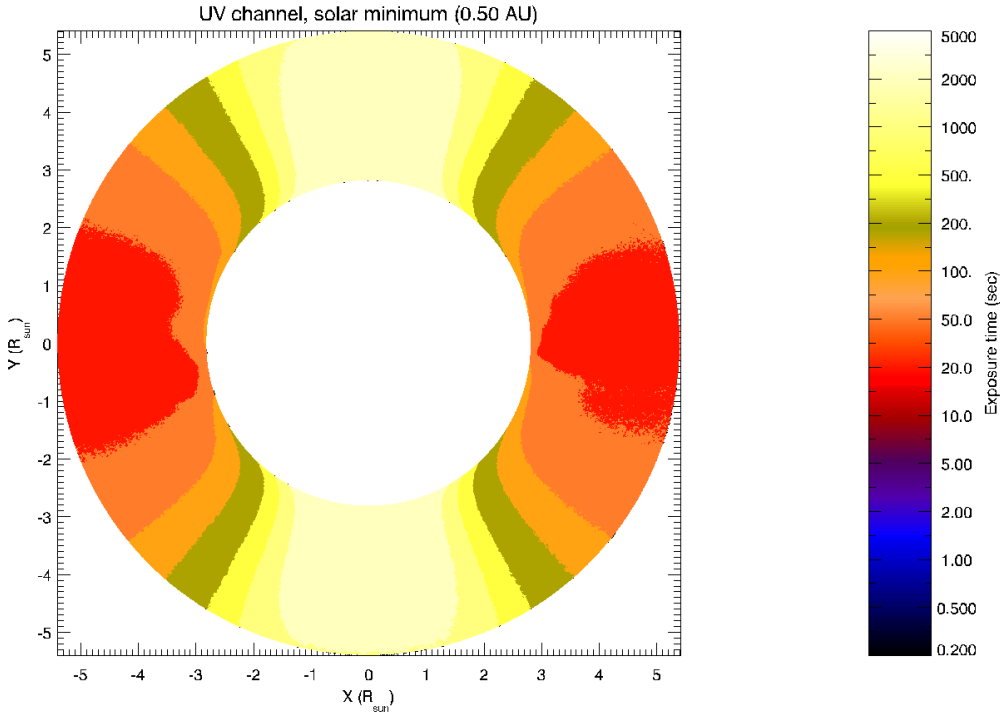
UV channel, solar minimum (0.50 AU)
Y (R sun)
X (R sun)
Exposure time (sec)
5000
2000
1000
500.
200.
100.
50.0
20.0
10.0
5.00
2.00
1.00
0.500
0.200

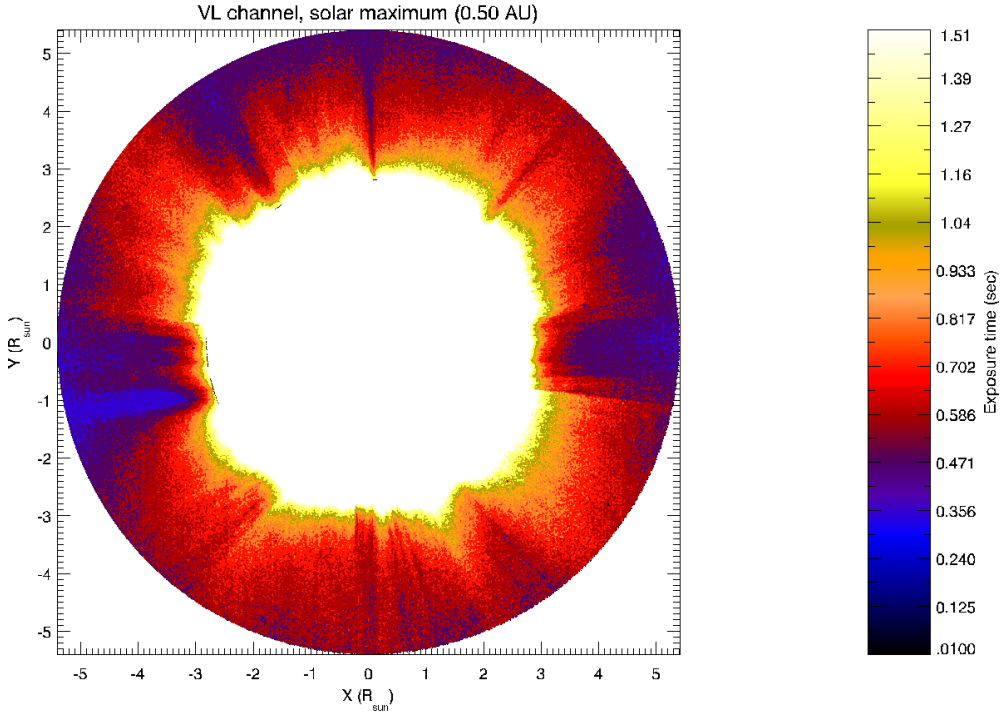
VL channel, solar maximum (0.50 AU)
Y (R sun)
X (R sun)
Exposure time (sec)
1.51
1.39
1.27
1.16
1.04
0.933
0.817
0.702
0.586
0.471
0.356
0.240
0.125
.0100

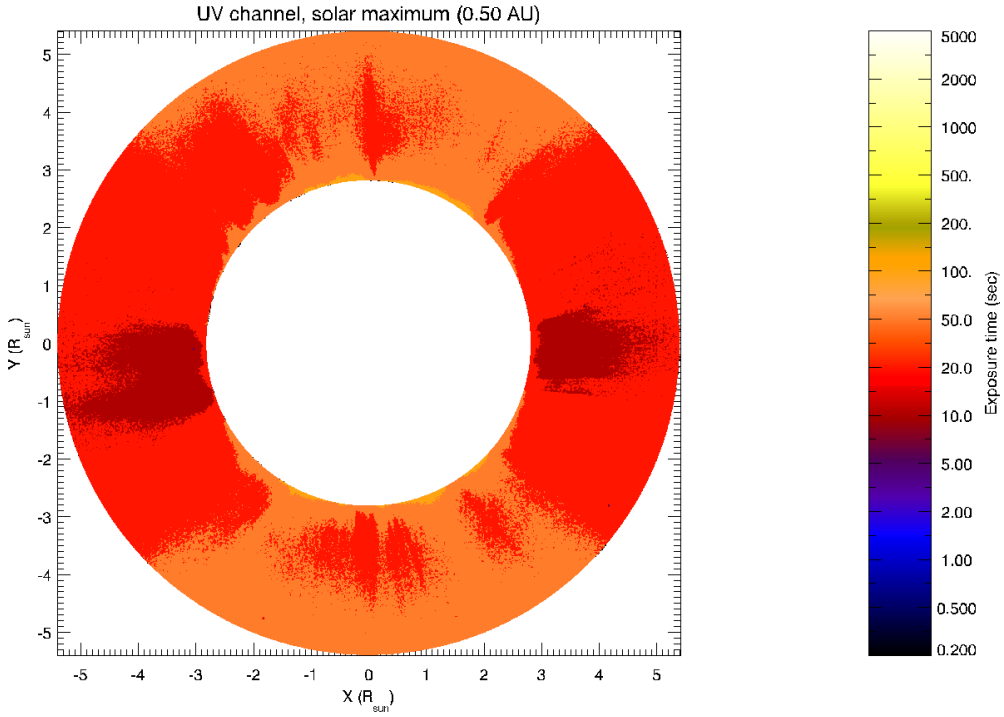
UV channel, solar maximum (0.50 AU)
Y (R sun)
X (R sun)
Exposure time (sec)
5000
2000
1000
500.
200.
100.
50.0
20.0
10.0
5.00
2.00
1.00
0.500
0.200